INL/RPT-22-68098-Revision-0

Bi-metallic Nanoparticle Synthesis for Advanced Manufactured Melt Wires

July 2022

Nicholas Alexander Der Garabedian, Kiyo T Fujimoto, Kennalee Orme

Changing the World's Energy Future

INL is a U.S. Department of Energy National Laboratory operated by Battelle Energy Alliance, LLC

INL/RPT-22-68098-Revision-0

Bi-metallic Nanoparticle Synthesis for Advanced Manufactured Melt Wires

Nicholas Alexander Der Garabedian, Kiyo T Fujimoto, Kennalee Orme

July 2022

Idaho National Laboratory
Idaho Falls, Idaho 83415

http://www.inl.gov

Prepared for the
U.S. Department of Energy
Under DOE Idaho Operations Office
Contract DE-AC07-05ID14517

Bi-metallic Nanoparticle Synthesis for Advanced Manufactured Melt Wires

Nicholas A. Der Garabedian[1,2] and Kiyo T. Fujimoto[1]

July 2022

[1]Idaho National Laboratory
[2] Villanova University

Abstract

Additive manufacturing (AM) based on direct-write technologies has emerged as the predominant method for the fabrication of passive sensors for the harsh operating environments seen in a nuclear reactor. Through the modification of previous methods, Idaho National Laboratory and Villanova University have improved the synthesis process for AM feedstock, which will allow for the improvement of advanced nuclear sensors and instrumentation. A major part of this work includes the synthesis process of relevant AM compatible feedstock to support the development, fabrication, and testing of AM sensors for peak temperature detection. For this report, bismuth, bismuth/platinum, tin, tin/silver, tin/zinc, indium, and indium/silver bi-metallic nanoparticles were synthesized using the polyol method, which will enhance temperature sensitivity and allow for miniaturization. To characterize the synthesized nanoparticles, we used x-ray fluorescence to evaluate the elemental composition of the nanoparticles and differential scanning calorimetry and thermogravimetric analysis to determine the melting point and mass loss of the samples. Results show that bi-metallic nanoparticles are a viable option for the fabrication of high-resolution AM melt wires. The temperature sensitivity can be brought to within 5˚C and melt wires can be fabricated that are in the micrometer scale. This will expand the range of irradiation experiments melt wires can be used for and the measured temperature will be significantly more accurate.

1. INTRODUCTION

Additive manufacturing (AM) has become the dominant method for innovation as it opens new opportunities in terms of design, materials, production, and functionality.[1] This style of manufacturing enables rapid prototyping, reduced production cost, and reduced material waste in comparison to typical manufacturing methods.[2] Essentially, AM takes on a new method of manufacturing, one that continues to add material layer by layer until the desired product is formed, rather than starting with raw material and removing material until a product is formed.[3] There are multiple styles of AM, each with strengths and weaknesses regarding the material used and functionality of the product. As part of the AM focus of the Nuclear Energy Enabling Technologies Advanced Sensors and Instrumentation Program (NEET ASI), the Idaho National Laboratory (INL) has made progress towards establishing unique capabilities to develop, produce, and test new additive-manufactured sensors that measure the peak temperature within a material test reactor during an irradiation experiment.[2] The ability to produce miniaturized and better performing sensors is possible through additive manufacturing techniques known as direct-write (DW) technologies.[4] These technologies include aerosol jet-printing, plasma-jet printing, inkjet printing, and micro-dispense printing.[5] Incorporating additive manufacturing expands the library of materials available for sensor fabrication. Furthermore, it is possible to fabricate sensors having geometries that are not otherwise possible with classical fabrication methods. The miniaturization of sensors will allow for the incorporation of melt wires into more experiment designs while also freeing up space to integrate more sensors in a given area, providing a better understanding of the reactor environment during testing.[6]

Currently, there are multiple different ways to measure the peak temperature passively and actively in a material test reactor. Active methods include High Temperature Irradiation Resistant Thermocouples which give temperature data in real time throughout the duration of an experiment.[7] However, peak temperature is generally monitored via passive techniques such as melt wires. To have an accurate temperature reading using melt wires, multiple are placed in an encapsulation. After predicting the peak temperature of the experiment, the melt wires are then placed into the irradiation capsule, some with melting points below and some above the expected peak temperature. After the experiment is complete, the melt wires are examined and depending on which have melted, the peak temperature can be inferred. At the present time, classical melt wire materials are obtained commercially and melt wire encapsulation is done in house at INL.[8]

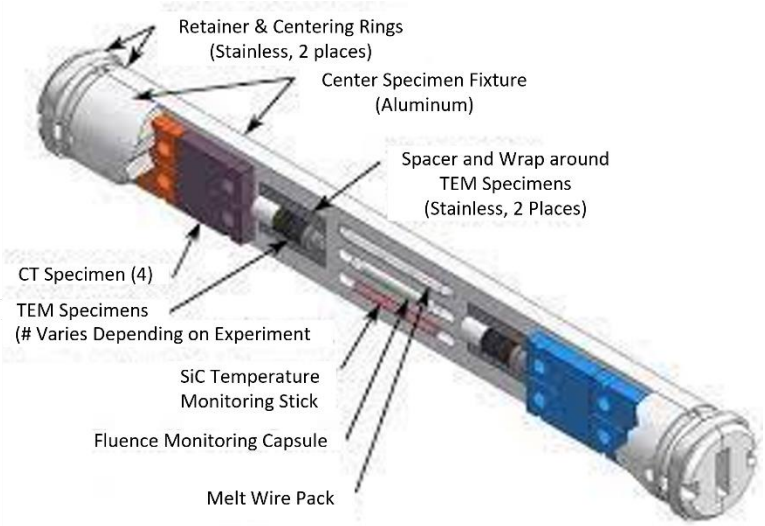

FIG. 1. Typical center fixture[8]

FIG. 2. Classical melt wire encapsulation[9]

Ideally, peak temperature measurements would provide a temperature resolution of less than 5˚C. However, this currently cannot be done with the limited selection of classical melt wire materials commercially available. On top of this, additively manufactured feedstock for melt wire fabrication is limited commercially. Therefore, incorporating additive manufacturing methods for additively manufactured melt wire fabrication requires the development of feedstock materials. This is the motivation behind developing in-house synthesis capabilities. These efforts in feedstock development for the NEET ASI program is to expand the library of materials available for AM technologies to enable the integration of additive manufacturing methods for melt wire fabrication. Developing feedstock production capabilities in-house enables the synthesis of unique material compositions for melt wires. This will significantly improve the performance of melt wires by enhancing the peak temperature monitoring resolution to within 5°C, which is considerably more accurate when compared to current gaps that have ranges upwards of 176°C[10].

Table 1: Current list of materials for classical melt wires[2]

Material (wt% of components)	Melt Onset (°C)	
56.2Bi33.8Pb10Sn	85.0	
65Bi35In	110.6	
55.2Bi44.8Pb	126.4	
57Bi43Sn	139.4	Δ92.4 °C
100Sn	231.8	
95Sn5Sb	238.6	
90Pb10Sb	252.4	
80Au20Sn	279.5	
90Pb7.5Sn2.5Ag	290.0	
97.5Pb2.5Ag	302.9	
97.5Pb5Ag5Sn	304.0	
97.5Pb1.75Sn1.75Ag	309.3	
100Pb	327.5	
100Zn	479.6	
80Sb20Zn	507.8	Δ152.7°C
100Al	660.5	
49Ag16Cu23Zn7.5Mn4.5Ni	681.3	Δ169.4°C
40Ti20Zr20Cu20Ni	850.7	
98.2Cu1.8Be	865.1	
100Ge	938.3	
82Au18Ni	955.0	
100Ag	961.9	
65Cu35Au	995.6	
100Au	1064.0	
100Cu	1084.6	
70Cu30Ni	1191.0	Δ176.0°C
28Mo69Ni2Pe1Co1Cr	1370.0	
100Ni	1455.0	

For this work, single and multicomponent metal nanoparticles were synthesized of bismuth, bismuth/platinum, tin, tin/zinc, tin/silver, indium, and indium/silver. Nanoparticle characterization was accomplished with the use of Differential Scanning Calorimetry (DSC) combined with Thermogravimetric Analysis (TGA), and X-Ray Fluorescence (XRF) to assess their potential for use as additively manufactured melt wire feedstock materials. These single and multicomponent metal nanoparticles were chosen because they are not commercially available. Due to the limited availability

of feedstock materials and inks available for DW technology, a major focus of this project and of the NEET ASI program is the development of unique feedstock to enable the fabrication of advanced sensors for in-pile application.

Melt wires are readily used in a material test reactor to measure peak temperature during irradiation testing.[11] Irradiation testing is used to better understand radiation-induced phenomena, such as the performance of fuels and materials in a harsh, nuclear environment.[5] Understanding the performance of these fuels and materials is critical to ensure safety and reliability while they are used in a reactor setting. Currently, melt wires are used in static capsule experiments. Static capsule experiments are self-contained, sealed experiment encapsulations that surround the specimen in an inert gas environment[12]. These capsules include passive instrumentation including melt wires, making the removal from and replacement into the reactor vessel efficient. Although they do not give real time readings, using passive sensors is the cheapest and quickest way to carry out an irradiation test. They are rather easy to replace and do not require the use of leads, which increases the cost of experiments significantly.[13]

The use of sensors within an irradiation experiment creates a stronger understanding of the reactor environment and radiation response to the material of interest. Using AM technology to produce unique and miniaturized melt wire sensors in-house will support a wider range of radiation experiments.[14]

2. MATERIALS AND METHODS

2.1 Materials

Single and multicomponent metal nanoparticles were synthesized using the following materials: diethylene glycol (DEG) (Reagent Plus 99%, Sigma Aldrich), sodium borohydride (99.99 trace metal basis, Sigma Aldrich), bismuth acetate (99.99%, Sigma Aldrich), polyvinylpyrrolidone (Sigma Aldrich), zinc acetate (99.99% trace metals basis, Sigma Aldrich), tin acetate (99.99%, Sigma Aldrich), silver nitrate (99.9999%, Sigma Aldrich), hexachloroplatinate acid (99.9999%, Sigma Aldrich), bismuth chloride (99.99%, Sigma Aldrich), and indium chloride (99.999% trace metals basis, Sigma Aldrich). Materials used for the XRF included Dow Corning high vacuum grease and a quartz disc for each sample. DSC/TGA was conducted with alumina crucibles (DSC Consumables, 6.5mm x 4mm). For the purification process, centrifuge tubes were used to hold the suspension of nanoparticles. The metallic pellet was resuspended in ethyl alcohol (>99.5%, Sigma Aldrich) and acetone (Spectrum) throughout the purification process. All chemicals and reactants were used as received, without further modification.

2.2 Methods

2.2.1 Nanoparticle Synthesis and Purification

Nanoparticle synthesis was accomplished using a method described previously, with modifications.[2] Tables 1-4 provide an overview for the entire bi-metallic nanoparticle series that was synthesized, which includes bismuth/platinum, indium/silver, tin/silver, and tin/zinc. To begin, 100 mL of diethylene glycol (DEG) was degassed within a three-neck round bottom flask. The degassing was done under reflux by bringing the solvent up to 200˚C while purging under high argon flow for a minimum of two hours. The DEG was allowed to cool to room temperature before adding

polyvinylpyrrolidone (PVP). Alongside, the metal salt precursors were dissolved in 10 mL of DEG. Next, sodium borohydride was dissolved in the vigorously stirring DEG and PVP solution and after ten minutes the metallic precursor solution was added dropwise (1 drop/sec) into the diethylene glycol, PVP, and sodium borohydride solution. After the entirety of the metal salt solution was added, the suspension was allowed to stir overnight.

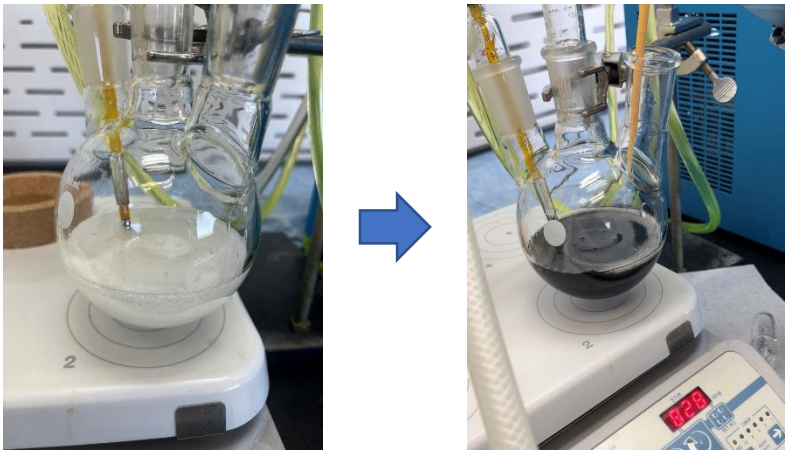

FIG. 3. Pre addition of metallic precursors (left) and post addition of metallic precursors (right)

Purification of nanoparticles to include removal of excess PVP capping agent and reaction by-products was accomplished with centrifugation. The processing parameters were as follows: each suspension of nanoparticles was transferred into a centrifuge test tube and placed into the centrifuge (Thermo Scientific, Legend XT). The samples were run at 9000 RPMs for 5 minutes. After each run, the supernatant was discarded, the pellet resuspended with ethanol, and the sample placed back in the centrifuge to run again. This was repeated for a minimum of five times per sample to ensure the removal of reaction by-products.

Table 1: Bismuth-Platinum series (1).

Nanoparticle System	Composition (at.%)	Bismuth (III) Acetate (g)	Hexachloroplatinic Acid (g)	PVP (g)	$NaBH_4$ (g)	DEG (mL)
Bismuth: Platinum	1:0	2.97	-	4.00	0.102	100
Bismuth: Platinum	95:5	0.881	0.058	4.00	0.101	100
Bismuth: Platinum	90:10	0.837	0.117	4.00	1.00	100

Table 2: Tin-Silver and Tin-Zinc series.

Nanoparticle System	Composition (at.%)	Tin (III) Acetate (g)	Zinc (III) Acetate (g)	Silver (III) Acetate (g)	PVP (g)	$NaBH_4$ (g)	DEG (mL)
Tin: Silver	1:0	0.592	-	-	0.014	0.500	100
Tin: Silver	96.5:3.5	0.518	-	0.014	0.151	0.502	100
Tin: Zinc	91:9	0.562	0.043	-	0.151	0.499	100

Table 3: Indium-Silver series.

Nanoparticle System	Composition (at.%)	Indium (III) Chloride (g)	Silver (III) Acetate (g)	PVP (g)	$NaBH_4$ (g)	DEG (mL)
Indium: Silver	1:0	0.5610	-	1.0363	1.0113	100
Indium: Silver	80:20	0.4439	0.0857	1.0099	1.0124	100
Indium: Silver	70:30	0.3995	0.1200	1.0019	1.0031	100

Table 4: Second Bismuth-Platinum series (2).

Nanoparticle System	Composition (at.%)	Bismuth (III) Chloride (g)	Hexachloroplatinic acid (g)	PVP (g)	$NaBH_4$ (g)	DEG (mL)
Bismuth: Platinum	1:0	0.7913	-	0.6053	0.2564	100
Bismuth: Platinum	95:5	0.7518	0.0619	0.6061	0.2554	100
Bismuth: Platinum	90:10	0.7131	0.1234	0.6092	0.2578	100

2.2.2 XRF

After the purification of each series was complete, the samples were prepared for the XRF. Each sample was removed from its test tube and placed into a plastic, sealed container. The samples were then dried in an oven to remove any leftover supernatant and placed onto a quartz disc. In order for the sample to stick on the quartz disc, a thin layer of vacuum grease was spread onto the discs to allow for an adhesive surface. After coating with vacuum grease, a small amount of sample was placed onto the disc, no more than a hair length in thickness. When each disc was coated with vacuum grease and held a sample, they were placed on an XRF cartridge. The cartridge was then loaded into the XRF (XFlash 660 SAR TXRF, Bunker) and set to run. For this experiment, no standard was used, and each sample was scheduled to run for 1,000 seconds, totaling 9,000 seconds for the nine samples that were tested. However, due to the added dead time, the test was run overnight and analyzed the following day. After

the test was complete, the composition of the particles on the discs were given. In each result, silicon was identified as >50% of the composition. However, this was due to the vacuum grease, which is made up of silicon. After accounting for all of the elements that were detected, the target metal compositions were converted to atomic percentages, allowing for the comparison of the predicted composition and the experimental.

2.2.3 DSC/TGA

In order to test the melting point of each sample, DSC was used. DSC detects endothermic and exothermic transitions, including the determination of transformation temperatures and the enthalpy of solids and liquids as a function of temperature. With the temperature constantly fluctuating, TGA was used to detect mass lost throughout the testing period. Each sample lost only a small percentage of mass, which accounted for the left over capping agent burning off during the initial heating period. The capping agent (PVP) has a far lower melting point compared to the rest of the samples, which allowed it to sublime during the initial heating period. Prior to testing, the melting point of each bi-metallic sample was predicted through the correlation between its composition and where that composition matches on the respective phase diagram. To prepare, between 5 and 50 milligrams of sample was loaded into a crucible. The crucible was closed and placed in the DSC/TGA (STA 449 F3, Netzsch) to run. In order to determine the melting point, a profile was developed for the DSC that specified at what temperature the DSC should start and end recording data, along with how many data points to take between each temperature range. Each sample ran overnight, and the experimental melting point was identified, along with the percentage of mass lost, after the run was completed.

3. RESULTS AND DISCUSSION

3.1 XRF

After running nine total samples in the XRF, the data was converted to atomic percent and compared to the theoretical atomic percent that was predicted. To convert the results to atomic percentages, 100 grams was assumed. Based off that assumption, the given weight percent of the target elements was converted directly to grams. The amount of grams of each target metal was multiplied by the molar mass to convert to the amount of moles of each target. Finally, the moles of each respective target metal were divided by the total amount of target metals in the system (in moles). After multiplying this result by 100, the atomic percent was given. The experimental compared with the theoretical atomic percentages of each system are shown in the table below:

Table 5: XRF Data – Theoretical vs. Experimental

Nanoparticle System	Theoretical Composition (at %)	Experimental Composition (at %)
Tin: Zinc	91:9	98.47: 1.53
Tin: Silver	96.5:3.5	98.40: 1.60
Tin: Silver	1:0	100: 0
Bismuth: Platinum	1:0	100: 0
Bismuth: Platinum	95:5	95.02: 4.98
Bismuth: Platinum	90:10	90.29: 9.71
Indium: Silver	1:0	100: 0
Indium: Silver	80:20	90.70: 9.30
Indium: Silver	70:30	77.4: 22.6

After the data was analyzed, it was clear that nanoparticle systems with only one target component had experimental compositions that were in complete agreement with the theoretical predictions, with only negligible differences due to contaminants. The series that alloyed best was the bismuth: platinum series, with extremely accurate results compared with the 95:5 and 90:10 theoretical compositions. The indium and tin series had results that did not agree well with the theoretical predictions, indicating that the bimetallic systems within these series did not alloy as well and both metal components were not as evenly distributed. This can be due to a variety of reasons, including the synthesis process. A stronger reducing agent may be needed in order to reduce the silver and zinc components within the indium and tin series because those metals have considerably higher reduction potentials compared to the indium and tin. With the current reducing agent, it is plausible to say that the metallic ions did not fully reduce and gain the electrons required to facilitate nanoparticle formation.

3.2 DSC/TGA

After running four samples through DSC/TGA, the melting point of the nanoparticle systems were determined. Using each material's respective phase diagrams, the theoretical melting point of each bimetallic system could be predicted and compared to the experimental melting point determined with DSC. The theoretical compared with the experimental melting point for each system tested is provided in Table 6:

Table 6: DSC/TGA Data – Theoretical vs. Experimental

Nanoparticle System	Composition (at %)	Theoretical Melting Point (˚C)	Experimental Melting Point (˚C)
Indium: Silver	1:0	156.6	157.3
Tin: Silver	1:0	231.9	230.3
Tin: Silver	96.5:3.5	221.0	219.4
Tin: Zinc	91:9	199.0	231.8

As shown, both single metal nanoparticle systems had experimental melting points that agreed with theoretical predictions, showing strong accuracy. The tin: silver system with a theoretical composition of 96.5:3.5 also showed strong accuracy, with the experimental melting point falling within 2˚C of the theoretical prediction. However, the tin: zinc system did not follow the pattern, showing far less accuracy when compared to the theoretical prediction. The experimental melting point was over 30 ˚C higher than the theoretical prediction, which indicated the melting point of pure tin rather than a tin/zinc alloy. Again, this can be accounted for a variety of reasons, including the synthesis process. As described above, a stronger reducing agent may be required in order to reduce the zinc ions to a zero valence state, which will allow for nanoparticle formation. However, inaccuracy can also be due to the purification process and any possible contaminants

TGA data identified any mass loss that occurred during the DSC testing. Mass loss was typically due to any excess PVP capping agent left on the synthesized nanoparticles. When the sample was run through DSC testing, the capping agent burned off during the first heating cycle, accounting for the loss in mass. Further, any excessive mass loss observed could also be accounted for material that was vaporized due to high temperature.

3.3 Future Work

The next steps of the project include completing DSC/TGA analysis for the remaining five samples. After this data is taken, future nanoparticle synthesis will be conducted, including an indium/platinum series. The long term goal is to use additive manufacturing to print the nanoparticles into wire form, creating functioning melt wires.

Acknowledgement

We would like to thank Harry Rollins for his support in collecting DSC/TGA data.
This work was supported through the Department of Energy Nuclear Energy Enabling Technologies Advanced Sensors and Instrumentation Program, under DOE Idaho Operations Office Contract DE-AC07-05ID14517, and under the Science Undergraduate Laboratory Internships Program (SULI).

References

[1] T.D. Ngo, A. Kashani, G. Imbalzano, K.T.Q. Nguyen, and D. Hui, Composites Part B: Engineering **143**, 172 (2018).

[2] K. Fujimoto and M. McMurtrey, (2021).

[3] T. Pereira, J. v. Kennedy, and J. Potgieter, in *Procedia Manufacturing* (Elsevier B.V., 2019), pp. 11–18.

[4] Y. Zhang, C. Liu, and D. Whalley, in *2009 International Conference on Electronic Packaging Technology and High Density Packaging, ICEPT-HDP 2009* (2009), pp. 497–503.

[5] K. Mondal, K. Fujimoto, and M.D. McMurtrey, JOM **72**, 4196 (2020).

[6] K.T. Fujimoto, L.A. Hone, K.D. Manning, R.D. Seifert, K.L. Davis, J.N. Milloway, R.S. Skifton, Y. Wu, M. Wilding, and D. Estrada, Sensors **21**, (2021).

[7] J.E. Daw, J.L. Rempe, D.L. Knudson, T.C. Unruh, B.M. Chase, K.L. Davis, and A.J. Palmer, *9.) Temperature Monitoring Options Available at the Idaho National Laboratory Advanced Test Reactor 9th International Temperature Symposium Temperature Monitoring Options Available at the Idaho National Laboratory Advanced Test Reactor* (2012).

[8] K.L. Davis and L.A. Hone, *7.) NSUF Melt Wire Evaluations for BSU-8242 and GE Hitachi-10393 Irradiation Experiments* (2020).

[9] J.L. Rempe, D.L. Knudson, J.E. Daw, T.C. Unruh, B.M. Chase, K.L. Davis, A.J. Palmer, and R.S. Schley, IEEE Transactions on Nuclear Science **61**, 1984 (2014).

[10] K.L. Davis, D.L. Knudson, J.E. Daw, J.L. Rempe, and A.J. Palmer, *8.) Melt Wire Sensors Available to Determine Peak Temperatures in ATR Irradiation Testing Eighth American Nuclear Society International Topical Meeting on Nuclear Plant Instrumentation, Control and Human-Machine Interface Technologies* (2012).

[11] K. Mondal, K. Fujimoto, and M. McMurtrey, *14.) Non-Visual Analysis of Miniaturized Melt Wire Arrays for in-Pile Measurement of Peak Irradiation Temperature* (2020).

[12] J.L. Rempe, D.L. Knudson, J.E. Daw, T.C. Unruh, B.M. Chase, K.L. Davis, A.J. Palmer, and R.S. Schley, IEEE Transactions on Nuclear Science **61**, 1984 (2014).

[13] S.B. Grover and R. v Furstenau, *5.) The Advanced Test Reactor Irradiation Facilities and Capabilities PHYTRA1: First International Conference on Physics and Technology of Reactors and Applications The Advanced Test Reactor Irradiation Facilities and Capabilities* (GMTR, 2007).

[14] J. Daw, J. Rempe, S. Taylor, J. Crepeau, and S.C. Wilkins, *16.) Ultrasonic Thermometry for In-Pile Temperature Detection NPIC&HMIT 2010* (2010).